Bioactive Materials 18 (2022) 1–14

Contents lists available at ScienceDirect

Bioactive Materials

journal homepage: www.keaipublishing.com/en/journals/bioactive-materials

Nanoenzyme engineered neutrophil-derived exosomes attenuate joint injury in advanced rheumatoid arthritis via regulating inflammatory environment

Lei Zhang [a,b], Ziguo Qin [c], Han Sun [a,b], Xiang Chen [a,b], Jian Dong [a,b], Siyu Shen [a,b], Liming Zheng [a,b], Ning Gu [c,**], Qing Jiang [a,b,*]

[a] State Key Laboratory of Pharmaceutical Biotechnology, Division of Sports Medicine and Adult Reconstructive Surgery, Department of Orthopedic Surgery, Nanjing Drum Tower Hospital, The Affiliated Hospital of Nanjing University Medical School, 321 Zhongshan Road, Nanjing, 210008, Jiangsu, PR China
[b] Branch of National Clinical Research Center for Orthopedics, Sports Medicine and Rehabilitation, PR China
[c] State Key Laboratory of Bioelectronics, Jiangsu Key Laboratory for Biomaterials and Devices, School of Biological Science and Medical Engineering, Southeast University, Nanjing, 210096, PR China

ARTICLE INFO

Keywords:
Engineered neutrophil-derived exosomes
Inflammation targeting
Inflammatory environment regulation
Effective treatment
Advanced rheumatoid arthritis

ABSTRACT

Rheumatoid arthritis (RA) is a chronic inflammatory disease characterized by synovitis and destruction of cartilage, promoted by sustained inflammation. However, current treatments remain unsatisfactory due to lacking of selective and effective strategies for alleviating inflammatory environments in RA joint. Inspired by neutrophil chemotaxis for inflammatory region, we therefore developed neutrophil-derived exosomes functionalized with sub-5 nm ultrasmall Prussian blue nanoparticles (uPB-Exo) via click chemistry, inheriting neutrophil-targeted biological molecules and owning excellent anti-inflammatory properties. uPB-Exo can selectively accumulate in activated fibroblast-like synoviocytes, subsequently neutralizing pro-inflammatory factors, scavenging reactive oxygen species, and alleviating inflammatory stress. In addition, uPB-Exo effectively targeted to inflammatory synovitis, penetrated deeply into the cartilage and real-time visualized inflamed joint through MRI system, leading to precise diagnosis of RA *in vivo* with high sensitivity and specificity. Particularly, uPB-Exo induced a cascade of anti-inflammatory events via Th17/Treg cell balance regulation, thereby significantly ameliorating joint damage. Therefore, nanoenzyme functionalized exosomes hold the great potential for enhanced treatment of RA in clinic.

1. Introduction

Rheumatoid arthritis is an autoimmune disease with chronic systemic inflammatory disorder, which is characterized by chronic synovitis that induces damage to articular cartilage [1–4]. Immune cells (T cells, macrophages, and neutrophils) and nonimmune (fibroblasts and chondrocytes) cells play an important role in the progression and prognosis of RA. Under the inflammatory microenvironment, immune cells participate in the secretion of many proinflammatory cytokines, chemokines and Matrix metalloproteinases (MMPs), thereby disturbing the immune balance and leading to cartilage and bone damage [2,4–6]. The current therapeutic approaches for RA aim to suppress the inflammation process, for example, by inhibiting the generation of inflammatory cytokines or clearing inflammatory cells from inflamed sites [7,8]. Although these treatments have generated substantial success, there is still more than 30% of RA patients exhibiting insufficient response to the first-line therapy [9–11]. Importantly, joint replacement has become the only choice for patients with advanced RA to restore joint function. Therefore, it is essential to develop novel therapeutic strategy with the potential to improve the efficacy for RA treatments.

Peer review under responsibility of KeAi Communications Co., Ltd.

* Corresponding author. State Key Laboratory of Pharmaceutical Biotechnology, Division of Sports Medicine and Adult Reconstructive Surgery, Department of Orthopedic Surgery, Nanjing Drum Tower Hospital, The Affiliated Hospital of Nanjing University Medical School, 321 Zhongshan Road, Nanjing, 210008, Jiangsu, PR China.
** Corresponding author.
E-mail addresses: guning@seu.edu.cn (N. Gu), qingj@nju.edu.cn (Q. Jiang).

https://doi.org/10.1016/j.bioactmat.2022.02.017
Received 14 September 2021; Received in revised form 14 February 2022; Accepted 14 February 2022
Available online 23 March 2022

Oxidative stress, a key component in the pathogenesis of chronic inflammation, implicated in the progression of RA [12–15]. Anti-oxidative agents, such as curcumin (Cur), lycopene and vitamin E, have the ability to reduce cartilage damage in RA animal models [6]. Unfortunately, their clinic applications were limited by low bioavailability, serious side effects, and expensive cost [16–20]. However, Prussian blue nanoparticles (PBNPs), as an antioxidative enzyme mimic, can effectively relief oxidative stress by catalyzing oxygen radicals [21,22]. Importantly, Prussian blue has been approved by the U.S. Food and Drug Administration (FDA) as a commonly used dye and medicine, suggesting its good biocompatibility and broad biomedical application [22,23]. Particularly, PBNPs can shorten the relaxation time of protons to enable their application as magnetic resonance imaging (MRI) contrast agents. Although PBNPs has promising antioxidative activities in the treatments of RA, its clinical application has been restricted due to the lack of specificity [25,26]. To overcome these defects of conventional drug treatment, it is necessary to develop a novel nanomedicine platform for effective RA therapy.

Currently, intelligent strategies for fostering restorative environment emerged as effective therapeutic interventions for the treatments of RA

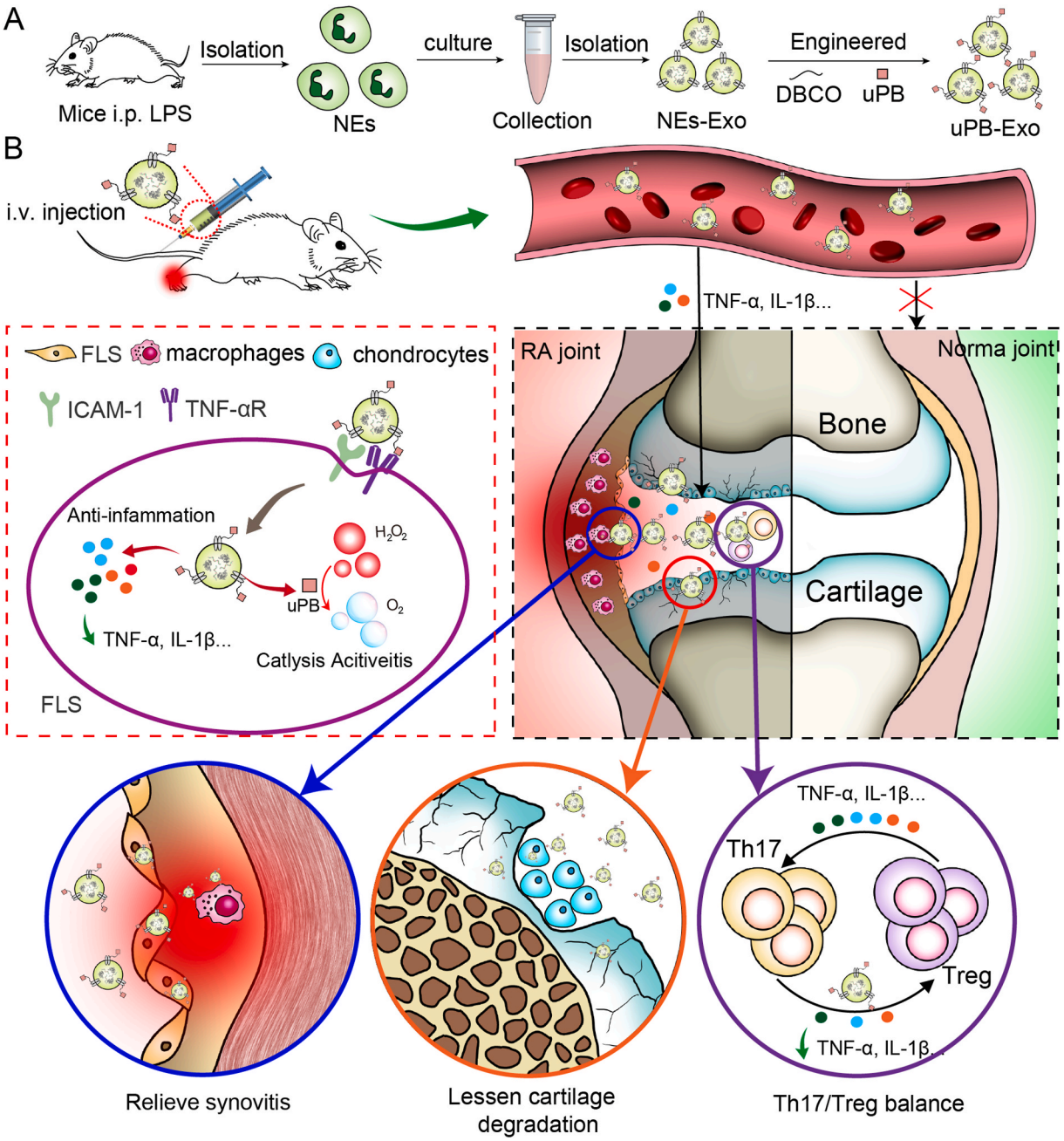

Fig. 1. Schematic illustration of nanoenzyme functionalized neutrophil-derived exosomes (uPB-Exo) mediated restoring inflammation environment for effective treatment of advanced rheumatoid arthritis. (A) uPB-Exo were developed by surface engineered neutrophil-derived exosomes (NEs-Exo) with sub-5 nm ultrasmall PBNPs (uPB) via click chemistry. (B) uPB-Exo can selectively accumulate in inflamed joints, and inhibiting the production of pro-inflammatory factors and alleviating inflammatory stress in activated fibroblast-like synoviocytes (FLS), macrophages and chondrocytes. In addition, uPB-Exo effectively targeted inflammation synovitis, penetrated deeply into the cartilage and real-time visualized inflamed joint in CIA mice *in vivo*, leading to diagnosis of RA with high sensitivity and specificity. Particularly, uPB-Exo showed significant therapeutic efficacy in RA by ameliorating joint damage and suppressing overall arthritis severity via inducing a cascade of anti-inflammatory events via Th17/Treg cell balance regulation.

[27]. During the progression of RA, neutrophils accumulate in the inflamed joints of RA at the early-stage of RA responding to inflammatory signals, and release pro-inflammatory cytokines (e.g. TNF-α, IL-1β, IL-6) resulting in continuous production of increased reactive oxygen species (ROS), leading to cartilage destruction and bone erosion [28]. Inspired by the critical roles in the initiation and progression of the disease, neutrophil based broad-spectrum anti-inflammatory strategy has emerged as a potent therapeutic strategy for RA. Zhang and the co-workers have developed neutrophil membrane-coated nanoparticles, which can neutralize proinflammatory cytokines, therefore inhibiting synovial inflammation and alleviating joint damage in inflammatory arthritis [29]. Meanwhile, Mauro Perretti and his group reported that neutrophil-derived MVs could decrease the production of stress-adaptive homeostatic mediators, thereby, lessening cartilage degradation caused by inflammatory arthritis [30]. Since neutrophil based anti-RA strategy have exhibited the therapeutic potential by decreasing proinflammatory cytokines, therefore, novel treatment strategy for attenuating inflammatory environments holds the great potential for the improvement therapy of RA.

Exosomes, 40- to 150-nm extracellular vesicles secreted by various kinds of cells, process the advantages of both synthetic carriers and cell-mediated carriers [31]. Previous studies demonstrate that exosomes can avoid the rapid clearance by the immune systems, minimize biotoxicity associated with synthetic vehicles, and even eliminate the unnecessary complexity in the applications of cell-mediated drug delivery systems in clinic [32]. Therefore, exosomes have the great potentials as a next-generation drug delivery vehicle. In addition, many issues have reported that exosomes possessed of anti-inflammatory effects, making it an alternative therapeutic agent for autoimmune diseases treatment [33]. Meanwhile, antioxidant therapy may offer novel complementary treatment options aiming at better controlling disease progression. For RA therapy, there is an unmet need to combine antioxidant and neutrophil derived exosomes, which can promote the synergistic effects of anti-inflammation for RA treatments.

Stimulated by our earlier successes in the development of neutrophil-mediated drug delivery system [34,35], here we attempted to develop a nanoenzyme functionalized neutrophil-derived exosomes to restore inflammatory environment in the inflamed joints of RA. In this study, we prepared a neutrophil-derived exosomes engineered with sub-5 nm ultrasmall PBNPs (uPB) via click chemistry, shortened for uPB-Exo, which can effectively achieve anti-inflammatory therapy for RA (Fig. 1A). uPB-Exo selectively accumulated in activated fibroblast-like synoviocytes, subsequently neutralizing pro-inflammatory factors and alleviating inflammatory environment (Fig. 1B). In addition, uPB-Exo can target inflamed joints of RA *in vivo*, and generating MRI images with good signal-to-noise. Particularly, uPB-Exo inhibits the production of pro-inflammatory factors and alleviates inflammatory stress, and consequently relieving inflammation synovitis and ameliorating cartilage damage via inducing Th17/Treg cell balance regulation in advanced RA mice model. Compared to current antirheumatic drugs, including anti-inflammatory drugs and biological antibodies [36–38], our anti-RA strategy owns prominent targeting ability for inflamed joint, which could improve therapeutic efficacy, shorten administrations times, and decrease unwanted side effects. Although nanotherapeutics have been developed for the treatment of RA with relatively reduced doses and side effects [39–41], uPB-Exo processes of almost no potential side effects derived from nanoenzyme (PBNPs) [22,23] or endogenous exosomes [42]. Most importantly, currently available RA mitigation drugs showed no obvious therapeutic effects for delaying the development of joint dysfunction in advanced RA [43,44], uPB-Exo could response to the increased inflammatory factors in the inflamed joints from RA mice with advanced arthritis, therefore scavenging reactive oxygen species and alleviating inflammatory stress. In summary, the engineered exosomes, as the inflammatory microenvironment regulator, has the great potential for facilitating RA diagnostic and therapeutic applications in clinic.

2. Materials and methods

2.1. Patient samples

The human peripheral blood samples, synovium, cartilage, and synovial fluid were obtained from three patients with late-stage RA patients (according to the American College of Rheumatology criteria) undergoing joint replacement surgery. The normal synovium, peripheral blood samples, cartilage, and synovial fluid were obtained from three patients with no synovitis and no cartilage injury as confirmed by arthroscopic examination. All samples were collected from Gulou Drum Tower Hospital Affiliated to the Medical School of Nanjing University. Informed consent was obtained from all patients, and ethical approval was obtained from the Ethics Committee of Gulou Drum Tower Hospital Affiliated to the Medical School of Nanjing University (approval No. 2020-156-01).

2.2. Neutrophils-derived exosome isolation

Lipopolysaccharide (LPS, 1.5 mg/kg) was injected intraperitoneally into the mice to activate neutrophils *in vivo*. Neutrophils were collected from bone marrow of mice after 6 h post injection, by Percoll gradient method described previously [34]. Neutrophils (10^7) were cultured in a 100-mm dish for 12 h in RPMI 1640 media and 10 mL supernatant were collected. Then neutrophils-derived exosomes were isolated from the harvested supernatant by using a supercentrifuge rotor. Briefly, the supernatant from neutrophils were centrifuged at 400 g for 10 min, 1250 g for 15 min, and 10,000 g for half an hour at 4 °C to remove cells and debris. After filtered using a 0.22-mm filter (Millipore, Billerica, MA, USA), the solution was centrifuged at 100,000 g for 70 min at 4 °C using an ultracentrifuge (Beckman Coulter, Brea, CA, USA). The exosome pellet was collected and resuspended in PBS, and ultracentrifuged again at 140,000 g for 70 min. Finally, the pelleted neutrophil-derived exosomes were obtained, and the protein quantification were determined by using a Micro BCA Protein Assay kit. To detect neutrophil marker (LFA-1, anti-IL-1R, anti-TNF-αR) and exosome markers (CD9, CD63 and TSG 101), western blotting was carried out with anti-LFA, anti-IL-1R, anti-TNF-αR, anti-CD9, anti-CD63 and anti-TSG 101 antibodies (Abcam, Cambridge, UK).

2.3. Preparation and characterization of azide modified prussian blue nanoparticles

PVP-modified Ultrasmall Prussian Blue Nanoparticles (uPB) were fabricated according to the reported procedure [45]. For the preparation of azide modified uPB, equal volume of uPB (1 mg/mL) and PAA solution (1.5 mg/mL) was mixed and stirred for 3 h. After removing excess PAA molecules using filters (100 kDa MWCO, Millipore), purified PAA@uPB was obtained. After stirring a mixture of PAA@uPB solution, PAH solution (3 mg/mL) and EDC solution (2 mg/mL) for 4 h at neutral environment (pH 7.4), the carboxyl groups from PAA and the amino groups from PAH on the surface of PB were chemically crosslinked. Then, PAH@PAA@uPB was obtained after purified with filters. Finally, azide modified Prussian blue nanoparticles N3@uPB was obtained after mixing PAH@PAA@uPB solution with Azidoacetic Acid NHS Ester solution (2 mg/mL in PBS) under sonication overnight at room temperature. After purified with filters, transmission electron microscope (JEOL, Tokyo, Japan) was employed to observe the morphology of PBs. The size distribution and zeta potentials of PBs were also measured using a Nano ZS90 device (Malvern). The ultraviolet–visible (UV–vis) absorption spectra of PBs were then obtained by a UV–vis spectrophotometer (UV-3600, Shimadzu, Japan).

2.4. Preparation and characterization of uPB-Exo

In order to prepare uPB-Exo, dibenzylcyclootyne (DBCO) groups

were introduced on the surface of exosomes using a hetero bifunctional crosslinker [46]. Briefly, dibenzocyclooctynesulfo-*N*-hydroxysuccinimidyl ester (DBCO-sulfo-NHS) (Sigma, St.Louis, MO, USA) was mixed with exosomes (0.5 mg/mL) in PBS solution on a rotating mixer at room temperature (RT) for 4 h. After removing extra DBCO-sulfo-NHS was through filters (Millipore), DBCO conjugated exosomes (DBCO-Exo) obtained for linking N3@uPB via copper-free click chemistry. Therefore, uPB-Exo were obtained, and the morphology was observed by Transmission electron microscope (JEOL, Tokyo, Japan). NTA was performed using a NanoSight NS300 system (Malvern). The size distribution and zeta potentials of exosomes were measured using a Nano ZS90 device (Malvern). Ultraviolet–visible (UV–vis) absorption spectra of uPBs were obtained by a UV–vis spectrophotometer (UV-3600, Shimadzu, Japan).

2.5. Measurement of magnetic resonance imaging (MRI) efficacy

The MRI assay was performed using a 7.0 T MR scanner (Biospec 7T/20 USR, Bruker, Germany). uPB-Exo (uPB concentration: 0.03125, 0.0625, 0.125, 0.25, 0.5, and 1.0 mM) and uPB solution with equal uPB concentration were used for T1 and T2 measurements. According to the T1 and T2 relaxation times, the values of longitudinal and transverse relativities (r1 and r2) were calculated to evaluate the contrast efficacy of samples.

2.6. Serum stability of uPB-Exo

Size distribution changes of uPB-Exo were evaluated after incubating in 50% Fatal Bovine Serum at 37 °C. Size and polydispersity index were measured at 1, 2, 4, 6, 8, 12 and 24 h by dynamic light scattering.

2.7. Cell culture

Primary mice chondrocytes, Fbroblast-like synoviocytes (FLS), or RAW 264.7 (ATCC) were cultured in DMEM medium (both from Cell Applications) at 37 °C in a 5% CO_2 environment.

2.8. Cellular uptake of uPB-Exo in activated FLS, chondrocytes and RAW 264.7 cells

FLS, chondrocytes or RAW 264.7 cells were seeded in 6-well culture plates. After cultured overnight, the culture medium was changed and LPS (2 μg/mL) was added for 6 h-stimulation, cells were washed with PBS and incubated with serum-free medium containing DiO-labeled NEs-Exo or uPB-Exo (Exosome 10^5 per well) for 2 h. After washed and stained by Hoechst, the cells were immediately observed using CLSM and the intracellular fluorescence intensity was measured using flow cytometry.

2.9. Measurements of cytokines level by ELISA

FLS, chondrocytes or RAW 264.7 cells were seeded in 6-well culture plates. After cultured overnight, the culture medium was changed, and LPS (2 μg/mL) or/and uPB-Exo (Exosome 10^5 per well) was added for 48 h. The supernatant was collected from culture media, and analyzed for the secretion of TNF-α or IL-1β using Elisa kit.

2.10. Measurement of ROS

FLS, chondrocytes or RAW 264.7 cells were seeded and incubated with stimulations (LPS 2 μg/mL) for 24 h uPB-Exo (Exosome 10^5 per well) were then added and incubated for 6 h. The intracellular levels of ROS in cells were stained by a ROS probe DCFH-DA. The cells were washed, and immediately observed using fluorescent microscope (Olympus), and the intracellular fluorescence intensity was measured using flow cytometry.

2.11. Cell viability assay

FLS, chondrocytes or RAW 264.7 cells were seeded and incubated with stimulations (LPS 2 μg/mL) for 24 h uPB-Exo were then added and incubated for 12 h. The cell viability was measured through CCK8 assay.

2.12. Live and dead cells assay

FLS, chondrocytes or RAW 264.7 cells were seeded and incubated with stimulations (LPS 2 μg/mL) for 24 h uPB-Exo (Exosome 10^5 per well) were then added and incubated for 12 h. The Live/Dead viability assay kit was used to observe apoptotic cell death. Fluorescence images were visualized under a confocal fluorescent microscope (Olympus).

2.13. Apoptosis evaluation

FLS, chondrocytes or RAW 264.7 cells were seeded and incubated with stimulations (TNF-α 100 ng/mL) for 24 h uPB-Exo (Exosome 10^5 per well) were pretreated for 4 h. The rates of cell apoptosis were determined using flow cytometry (FCM) analysis with an Annexin V-FITC/PI apoptosis kit.

2.14. RNA library construction and sequencing

After treated with TNF-α with or without uPB-Exo, total RNA was harvested from FLS, chondrocytes or Macrophage. The total RNA was extracted by TRIzol reagent (Invitrogen, CA, USA), and paired-end sequencing were performed on an Illumina HiSeq 4000 at LC-BIO Technologies (Hangzhou) Co., LTD by following the vendor's recommended protocol. cDNA library preparation and sequencing reactions were performed to unravel the crucial molecular regulator during uPB-Exo treatments in protecting FLS, chondrocytes, or Macrophage from cytokines.

2.15. Induction of collagen induced arthritis

DBA1/J mice were purchased from Model Animal Research Center of Nanjing University. All mice were kept under pathogen free and 12 h light/dark cycle conditions with enough food and water. The animal use and the experimental protocols were reviewed and approved by the Animal Care Committee of the Nanjing University in accordance with the Institutional Animal Care and Use Committee guidelines. CIA mouse model was established by following a previously published protocol [47]. Briefly, chicken CII (Condrex Inc., WA, USA) was emulsified with an equal volume of complete Freund's adjuvant (Sigma, MO, USA). DBA1/J mice were immunized via an intradermal injection at the base of the tail with 50 μL of emulsion (CII 100 μg/mouse) at 0 day and 21 days. Mice with 5 days of disease induction were stipulated as CIA mice with early-stage arthritis and an advanced arthritis mice model was successfully developed 15 days after disease induction.

2.16. In vivo imaging of engineered exosome in CIA mice

CIA mice were intravenously injected with DiR-labeled exosome (DiR@NE-Exo and DiR@uPB-Exo), fluorescence dye DiR was taken as control. Mice were anesthetized with isoflurane and images were taken by the IVIS Spectrum system (Caliper, USA) at 1, 2, 4, 8, 12 and 24-h post injection. The mice were euthanized, and paws as well as major organs were harvested and subjected for *ex vivo* imaging. Region-of-interests were circled around the organs, and the fluorescence intensity was analyzed by Living Image Software. To further confirm whether DiR@uPB-Exo was mainly accumulated in the cartilage region, the fresh joints were collected and immediately fixed in 4% PFA solution for 1 day, followed with the decalcification in 0.5 M EDTA at 4 °C with constant shaking for 5 days. Then, the joints were infiltrated with 25% sucrose phosphate buffer for 2 days. All samples were embedded in the

mixture of 25% sucrose solution and OCT compound (Leica) at the ratio of 1 : 1. The joints were cut into 10-μm-thick sagittal sections, and then stained with Collagen II antibody. Nuclei were stained with Hoechst (Beyotime Biotechnology), and images were taken by CLSM.

2.17. In vivo MR imaging of engineered exosome in CIA mice

T1-weighted MR images were collected using a 7.0-T 20-cm-bore MRI system (Bruker Biospin, Ettlingen, Germany) equipped with a mice brain surface coil (4 ch). T2-weighted MR images were acquired under inhalational anesthesia with isofluorane and at 1, 2 and 4 h after intravenous injection of uPB-Exo and uPB solution (150 μL, 0.5 mg/mL in PBS). T1 color map images were processed with the Image Sequence Analysis Tool of Bruker Paravision 5.1 (Bruker Biospin, Ettlingen, Germany).

2.18. Engineered exosomes penetration study

DiR-labeled Engineered exosomes (DiR@NE-Exo or DiR@uPB-Exo) or DiR dye were incubated with the femoral heads pretreated with 10 ng/mL recombinant mouse IL-1β at 37 °C for 24 h. After washed with PBS, femoral heads were embedded in OCT Compound for frozen sectioning. The joints were cut into 10-μm-thick sagittal sections, and then stained with Collagen II antibody. Nuclei were stained with Hoechst (Beyotime Biotechnology), and images were taken by CLSM (Zeiss, Germany).

2.19. In vivo efficacy study

To evaluate therapeutic efficacy with CIA mice, 100 μL of engineered exosome uPB-Exo and NEs-Exo (Exosome 10^7 per mouse) was injected into each tail vein on days 0 (first day of obvious clinical signs of late-stage arthritis), 3, 6, 9, 12, 15, 18, and 21 days. Sterile PBS and PBNPs solution as negative control was injected intravenously to CIA mice on the same days. The arthritis index, weight, paw thickness and paw volume of each group was recorded over time. After 25 days of treatment, the mice were sacrificed, and the paw joints were collected for micro-computed tomography (micro-CT) analysis. Briefly, the paws of mice from the different groups were fixed for 24 h with 4% paraformaldehyde, then examined and analyzed using a micro-CT imaging system micro-CT scanner (Scanco Medical, Bruettisellen, Switzerland).

2.20. Histological analysis of mouse joints

At study endpoints, mice were euthanized and the joints were collected for H&E staining and safranin-O staining. In addition, the joint tissues sections were scored for changes in cell infiltration, bone erosion, and synovial proliferation, all on a scale of 0–4. The score was assessed and the average grades were calculated. To analyses fibroblast-like synoviocyte activation, knee joint sections were stained with a rabbit anti-IL-6, rabbit anti-TNF-α or a rabbit anti-IL-1β. Alexa Flour 594 labeled anti-rabbit IgG was used as the secondary antibody. Sections were counter-stained with to visualize cell nuclei. Frozen sections were stained by DAPI and imaged with confocal (Zeiss, Germany).

2.21. Quantification of inflammation cytokines

The serum samples from CIA mouse were collected on days 0 (first day of obvious clinical signs of late-stage arthritis), 5, 10, 15 and 20 days, and concentrations of IL-1β and TNF-α were quantified with ELISA according to the manufacturer's instructions.

2.22. Flow cytometry

Cells were isolated from the blood of arthritic mice after different treatments. The following fluorescence-conjugated mouse antibodies were used for flow cytometric analysis: from BioLegend (San Diego, CA, USA): mouse FITC-CD4, APC-CD25, PE/Cy7-Foxp3, PE-IFN-γ. Cell subset was analyzed on a FACS Calibur flow cytometer using Cell Quest Software (Becton Dickinson). For intracellular staining, including IFN-γ and Foxp3, cells were first stained with surface marker CD4, and further fixed and permeabilized for intracellular staining. Plot figures were prepared using FlowJo Software (Tree Star Inc., Ashland, OR, USA).

2.23. In vivo safety evaluation of exosomes in CIA mice

The safety of the exosomes was evaluated by examining the main organs via histological sectioning and H&E staining. Samples from untreated mice were used as controls.

2.24. Statistical assessment

SPSS 13.0 software (Statistical Package for the Social Sciences, USA) was used to analyze the obtained data, which are presented as the mean ± SD. Comparison between two groups was accomplished via an unpaired two-tailed student's *t*-test. $p < 0.05$ indicated a statistically significant difference.

2.25. The inflammatory microenvironment of joint from advanced RA patients

Rheumatoid arthritis (RA) is an inflammatory autoimmune disease, characterized by a highly coordinated inflammatory response which causes chronic synovitis and bone erosion [3]. At the initiation and progression of RA, neutrophils migrate into the articular cavity and become activated in response to inflammatory factors [30]. Activated neutrophils sequentially interact with normal FLS, and drive them into an inflammatory phenotype. To investigate the inflammatory microenvironment of RA patients, neutrophils associated inflammatory factors and chemokines in synovium tissue were measured by immunofluorescence analyses. As shown in Fig. 2A, synovium tissue from RA patients exhibited higher expression of inflammatory factors (TNF-α and IL-1β) and neutrophil Chemokines (IL-8) compared with normal patients (Fig. S1). In addition, obvious expression of neutrophil surface maker CD11b was detected in synovium tissue from RA patients, however, synovium tissue from normal patients exhibited negative staining of CD11b by immunofluorescence analysis (Fig. S1), suggesting that neutrophils play an important role in the development of RA.

Collected evidence have shown that the dysregulated inflammatory occurred in the synovium results in the destruction of both cartilage and bones of the joint [48], we therefore identified the distribution of neutrophil in cartilage and synovial fluid in RA patients. As show in Fig. 2B, noticeable number of neutrophils was observed in synovial fluid from RA patients compared to normal patients (Fig. S2). In addition, neutrophils, stained with Myeloperoxidase (MPO), a key neutrophil enzyme [49], can penetrate into RA articular cartilage deeply (Figs. 2C and S3). These results indicated that neutrophils can participate in the progression in RA patients with obvious cartilage destruction (Fig. S4). Since neutrophils act as mediators of inflammation, the concentration gradient of inflammation factor was further to explored in both serum and synovium in advanced RA patients by Elisa kit. As shown in Fig. 2D and E, the expression of inflammatory factors (TNF-α and IL-1β) and neutrophil Chemokines (IL-8) in RA patients were more than 4-fold, compared to normal people samples, suggesting that neutrophils can migrate to the inflammation joint responding to chemotactic factor generation conditions. Therefore, neutrophils associated dysregulated inflammatory occurred in the synovium, articular cavity, and cartilage of joints from RA patients.

2.26. Recruitment of NEs-Exo in advanced RA inflammation joint

Many issues have shown that the neutrophil activation could release

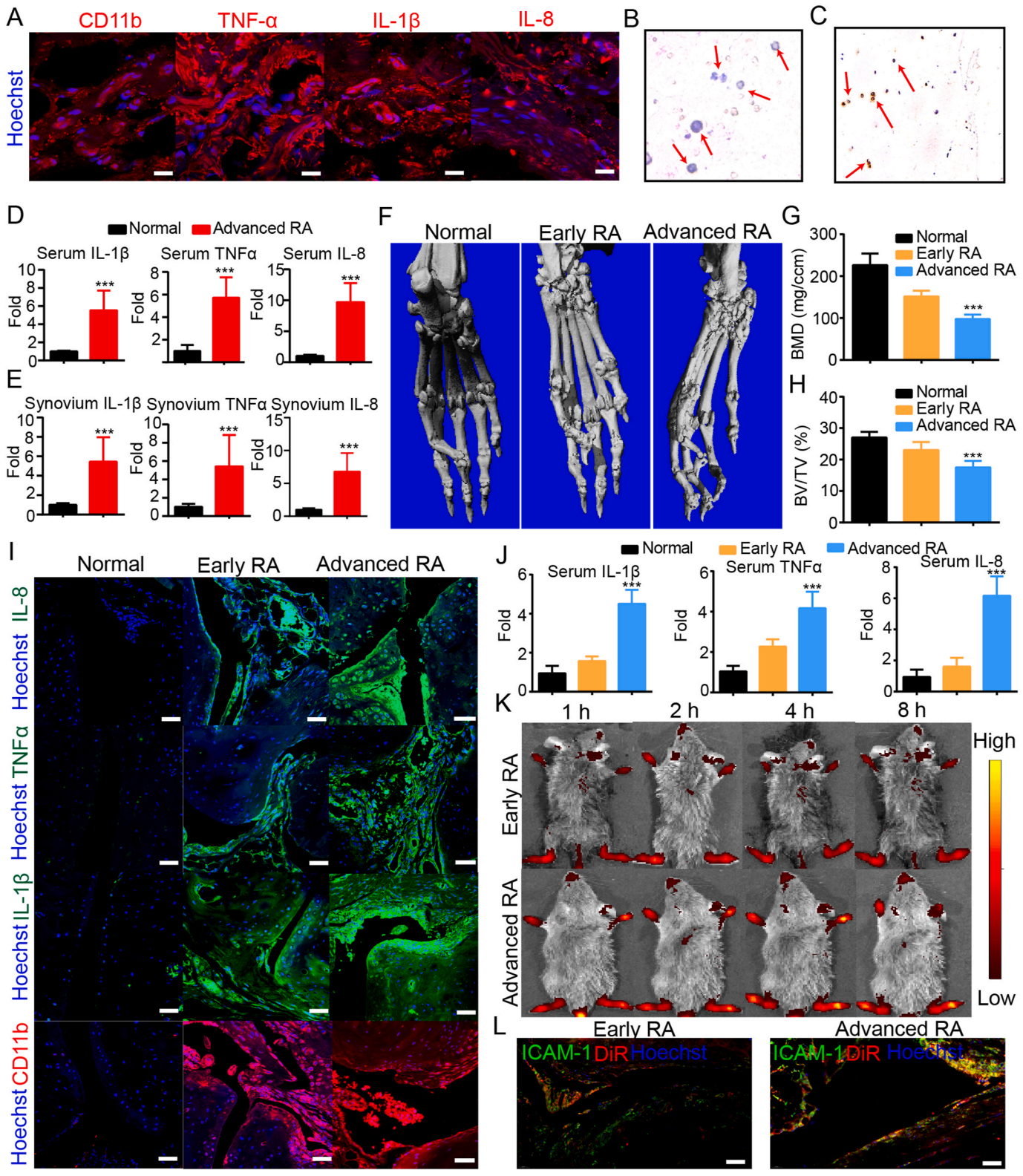

(caption on next page)

Fig. 2. Recruitment of NEs-Exo in inflamed joints from advanced RA responding to pathological inflammation. (A) Immunofluorescence analyses of CD11b, TNF-α, IL-1β and IL-8 in synovium tissue from RA patients. Scale bars indicate 20 μm. (B) Wright-Giemsa stain of neutrophil on synovial fluid from RA patients. Images were acquired at 10x magnification on an Olympus microscope. The red arrows indicate neutrophils. (C) IHC staining of MPO in cartilage from RA patients. Images were acquired at 10x magnification on an Olympus microscope. The red arrows indicate MPO-positive neutrophils. (D), (E). The concentration of inflammation factors (TNF-α, IL-1β and IL-8) in serum (D) and synovium tissue (E) from RA patients. (F) Representative micro-CT images of ankle joints from normal mice, CIA mice with early-stage arthritis, and CIA mice with late-stage arthritis. (G), (H) Quantitative micro-CT analyses of bone mineral density (BMD) and bone surface density (BS/BV) in ankle joints from normal mice, CIA mice with early-stage arthritis, and CIA mice with late-stage arthritis. (I) Immunofluorescence analyses of the TNF-α, IL-1β, IL-8 and CD11b in the joint tissues from normal mice, CIA mice with early-stage arthritis, and CIA mice with late-stage arthritis. Scale bars indicate 20 μm. (J) The concentration of inflammation factors (TNF-α, IL-1β and IL-8) in serum from normal mice, CIA mice with early-stage arthritis, and CIA mice with late-stage arthritis. (K) In vivo fluorescence images of DiR labeled NEs-Exo after i.v. injected with CIA mice with early-stage arthritis and late-stage arthritis within 8 h-post injection. (L) Immunofluorescence analyses of the ICAM-1 (green) and the fluorescence images of DiR labeled NEs-Exo (red) in the joint tissues from CIA mice with early-stage arthritis and late-stage arthritis. Scale bars indicate 20 μm. Data represent the mean ± SD (n = 3 independent samples). Statistical significance was determined by a two-sided Student's *t*-test. ***$p < 0.001$.

IL-1β, and stimulate macrophages and synoviocytes to express proinflammatory factors, which in turn amplify neutrophil recruitment. Subsequently, neutrophil activation would produce extra ROS and release MMPs, which causes cartilage destruction and bone erosion [28]. Therefore, the accumulation of extra neutrophil carriers in inflammation joints of RA has high risk for promoting the development and progression of RA. It has been reported that exosomes are nano-sized (30–100 nm) mammalian extracellular particles with essential properties in terms of cell communications [31]. Exosomes are cell-created vesicles that inherit identical phospholipid membrane [50]. Neutrophil membrane expressed the key surface antigens (including LFA-1, IL-1R and TNF-αR). Since the LFA-1 on the neutrophil membrane could bind with the intercellular activation molecule 1 (ICAM-1) overexpressed on activated FLS [51], chondrocytes [52] and macrophage [53], the targeting capability of NEs-Exo is probably attributed to the expression of LFA-1 derived from neutrophils [54,55]. Therefore, we conjectured that neutrophil transfer key surface antigens to their exosomes, thereby, neutrophils-derived exosomes (NEs-Exo) can response to the appeals of inflammation.

To explore the targeting ability of NEs-Exo in RA, a CIA mouse model, a well-characterized model for assessing the stages of pathology in RA and exploring arthritis mechanisms, is established. We therefore investigated joint destruction and synovial inflammation in CIA mice by using micro-computed tomography (micro-CT), immunofluorescence and Elisa assay. After scanned the ankle joints of mice by using Micro-CT, the smooth bone surface in ankle joints were observed in CIA mice with early-stage arthritis compared to normal ankle joints. In the contrast, CIA mice with advanced arthritis displayed apparent rough bone surfaces and significantly decreased bone mineral density (BMD) and bone surface density (BS/BV) (Fig. 2F, G and 2H) compared to normal ankle joints. Moreover, various chemoattractants, including TNF-α, IL-1β and IL-8, have been identified that promote neutrophil migration into inflammation ankle joint. Compared to early-stage arthritis, significant increased expression of chemoattractants were observed in CIA mice with late-stage arthritis (Fig. 2I and J). These results indicated that NEs-Exo has the great potential to be a potent target carrier for advanced RA. To assess the recruitment ability of NEs-Exo (Figs. S5 and S6) to advanced RA, *in vivo* imaging experiment were carried out in both early-stage arthritis and late-stage arthritis. As shown in Fig. 2K, we found that apparent red signal of DiR labeled NEs-Exo were observed in inflamed joints of CIA mice after 1 h-i.v. injection. Importantly, NEs-Exo exhibited notable accumulation in ankle joints region from advanced RA, generating a 2.4-fold higher in fluorescence intensity compared to early-stage arthritis (Fig. S7). In addition, we found that more ICAM-1(Green signal) were observed in late-stage arthritis compared to early stage (Fig. 2L). In addition, obviously DiR labeled NEs-Exo (red signal) accumulated in ICAM-1(Green signal) labeled inflamed ankle joints in late-stage arthritis, and the merged yellow signal were stronger than that in inflamed ankle joints in early-stage arthritis. These results indicate that NEs-Exo holds great potential as a target carrier for RA treatments. Considering that NEs-Exo showed no apparently inflammation-promoting ability (Fig. S8), NEs-Exo therefore holds the great promising in the diagnosis and treatment of advanced RA. Current RA mitigation drug show no obvious effects for delaying the development of joint dysfunction in advanced RA, hence, it is essential to develop novel therapeutic strategy with the potential to improve the efficacy for RA treatments.

2.27. Preparation and characterization of uPB-Exo

Increasing evidence have reported that oxidative stress, which can lead to chronic inflammation, plays a key role in the pathogenesis of RA [12]. Antioxidants therapies for RA were limited by low bioavailability, serious side effects, and expensive cost. Since exosomes, possessing of good biocompatibility, have been widely applied as a drug delivery system. Inspired by the excellent targeting ability of NEs-Exo for advanced RA and potential anti-inflammatory activity based neutrophil derived vesicles [30], we therefore functionalized NEs-Exo with sub-5 nm ultrasmall PBNPs (uPB-Exo) via "click chemistry", endowed it with mimic enzyme activities for ROS scavenging and visualization capability for magnetic resonance imaging. As show in Fig. 3a, uPB modified NEs-Exo (uPB-Exo) were obtained by linking the DBCO groups on the exosomes with azide-functionalized uPB (Fig. S9, S10 and S11) to form stable triazole linkages using copper-free click chemistry. NEs-Exo with average diameter of 116 nm and zeta potential of −25 mv displayed round and well dispersed appearance measured by TEM images. After engineered with uPB, the mean diameter of exosomes increased to 126 nm, and the zeta potential remained nearly unchanged for NEs-Exo (Fig. 3B and C). In addition, the UV-vis spectra showed obvious uPB peak at 694 nm, demonstrating that uPB were successfully coating at NEs-Exo (Figs. 3D and S12). Meanwhile, the size distributions of uPB-Exo were evaluated using NTA, which showed that the highest peak of both profiles were around 124 nm (Fig. 3E), which is consistent with DLS measurement. More importantly, we implemented HSFCM to determine the grafting ratio of uPB on NEs-Exo. Cy3-N_3 were modified into the surface of NEs-Exo according to the same method of uPB-Exo, therefore Cy3-Exo were obtained. The particle concentration of Cy3-Exo (with an Cy3 concentration of 0.1 mg/mL) was measured to be 1.98×10^{10} particles/mL. Based on the concentration and molecular weight of the Cy3, it was calculated that the NEs-Exo contained an average of ~378 Cy3-N3 per particle. These results indicated that NEs-Exo contained an average of ~378 uPB per NEs-Exo. Furthermore, the serum stability assay was conducted to investigate interactions between uPB-Exo and blood components. The average particle sizes remained nearly unchanged for NEs-Exo after 24 h of storage in 50% fetal bovine serum (FBS) at 37 °C (Fig. 3F), suggesting its good biostability. Importantly, WB experiments demonstrated the presence and enrichment of key surface antigens, including TNF-α receptor (TNF-αR), IL-1 receptor (IL-1R) and lymphocyte function-associated antigen-1 (LFA-1) on both uPB-Exo and NEs-Exo (Fig. 3G), confirming that the modification of uPB cannot affect the biofunction of NEs-Exo.

In our previously work, uPB exhibited good performance in POD- and CAT-like Catalytic activity [56], we therefore assessed the antioxidative ability of uPB-Exo to relief ROS. Fig. 3H displays that uPB-Exo

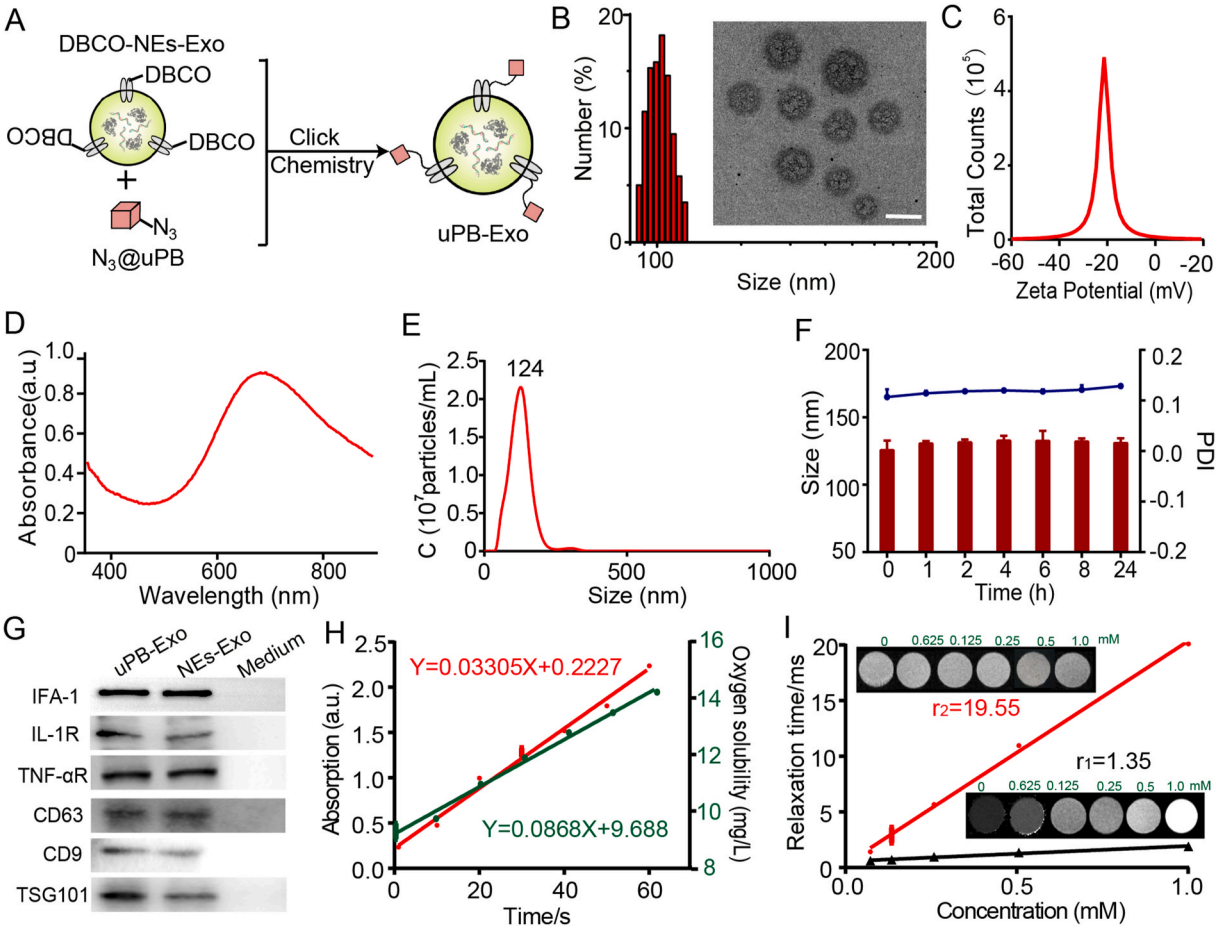

Fig. 3. Preparation and characterization of uPB-Exo. (A) Schematic representation of uPB-Exo designed for selectively suppressing inflammatory stress in RA joints. uPB-Exo are constructed by coating uPB on the surface of Neutrophil-derived exosome (NEs-Exo), which mimic source cells to bind with immunoregulatory molecules without potentiating the immune cascades for disease progression. (B) Hydrodynamic size of uPB-Exo measured by DLS. The insert image indicated the transmission electron microscopy images of uPB-Exo. Scale bar indicated 100 nm. (C) The zeta potential of uPB-Exo measured by DLS. (D) The UV–vis absorbance of uPB-Exo measured by Microplate Reader. (E) NTA distribution of uPB-Exo. (F) The serum stability of uPB-Exo in 50% Feta bovine serum within 24 h. (G) Western blots for Exo markers (CD63, CD9, TSG101) and neutrophil markers (LFA, IL-1R, TNF-αR) of uPB-Exo and NEs-Exo. Fresh Exo-free complete medium was used as control. (H) POD-like catalytic activity of uPB-Exo (Left longitudinal axis). CAT-like catalytic activity of uPB-Exo (Right longitudinal axis). (I) uPB concentration-dependent T1 and T2 relaxation rates of uPB-Exo. The insert indicated T1, T2-weighted MRI phantoms of uPB-Exo with various uPB concentrations. Data represent the mean ± SD (n = 3).

exhibits almost overlapped POD-(Fig. S13) and CAT-like Catalytic activity (Fig. S14) with uPB, implying that uPB-Exos has superior POD-like catalytic activity similar to uPB. As a multifunctional nanozyme, uPB can also act as CAT to catalyze the decomposition of H_2O_2 into O_2 and H_2O under neutral conditions. As shown in Fig. 3H, S13 and S14, uPB as well as uPB-Exo exhibited excellent catalytic activity even when its concentration (0.3 μg/mL). These results indicated that uPB-Exo exhibited an intensive ability of decomposing hydrogen peroxide to generate oxygen, scavenging free radicals, and protecting cells from being oxidized. Therefore, uPB-Exo could effectively scavenge free radicals and owned great application potential in the antioxidative treatment for RA.

Prussian blue nanoparticles can influence the longitudinal and transverse relaxation times of protons from water as T1 contrast agent [56]. In this study, a 7.0 T MRI system was used to measure a series of proton T1 relaxation times. The T1-weighted MRI slices of phantoms consisting of uPB and uPB-Exos with various uPB concentrations are displayed in Fig. 3I, the longitudinal and transverse relaxation rates (r1 and r2) could be measured with the linear slopes of 1/T1 and 1/T2 versus the uPB concentration, respectively (Fig. S15). In addition, the r2/r1 ratio of uPB was calculated, which was similar as uPB-Exo. These results demonstrated that uPB-Exo could act as an effective T1 contrast agent for the diagnosis of RA in clinic.

2.28. *Inflammatory environment regulation of uPB-Exo in vitro*

The activation of fibroblast-like synoviocytes (FLS) in the inflamed synovium contribute to cartilage destruction through their production of inflammatory cytokines and chemokines [1,2]. We therefore take activated FLS as RA cell models to investigate the distribution behaviors of various prepared exosomes in inflamed joint *in vitro*. The fluorescent probe DiO, was used to labeled uPB-Exo, and intracellular uptake were measured through Confocal laser scanning microscope (CLSM) and flow cytometry. As shown in Figs. 4A and S16, uPB-Exo and NEs-Exo can selectively accumulate in cytokine activated FLS compared to normal cells, suggesting that uPB-Exo could selectively target cytokine activated FLS. In addition, flow cytometry measurements confirmed that significant increase in mean fluorescence intensity (MFI) in activated FLS after incubated with uPB-Exo, which is 3.1-fold compared to normal FLS (Fig. S17). The selectivity of uPB-Exo in activated Chondrocyte and RAW264.7 cells were also observed in Fig. 4A and B. These results demonstrated the good targeting ability of uPB-Exo for inflamed RA-associated cells. The specific binding was probably attributed to specific interactions between LFA-1 on the surface membrane of

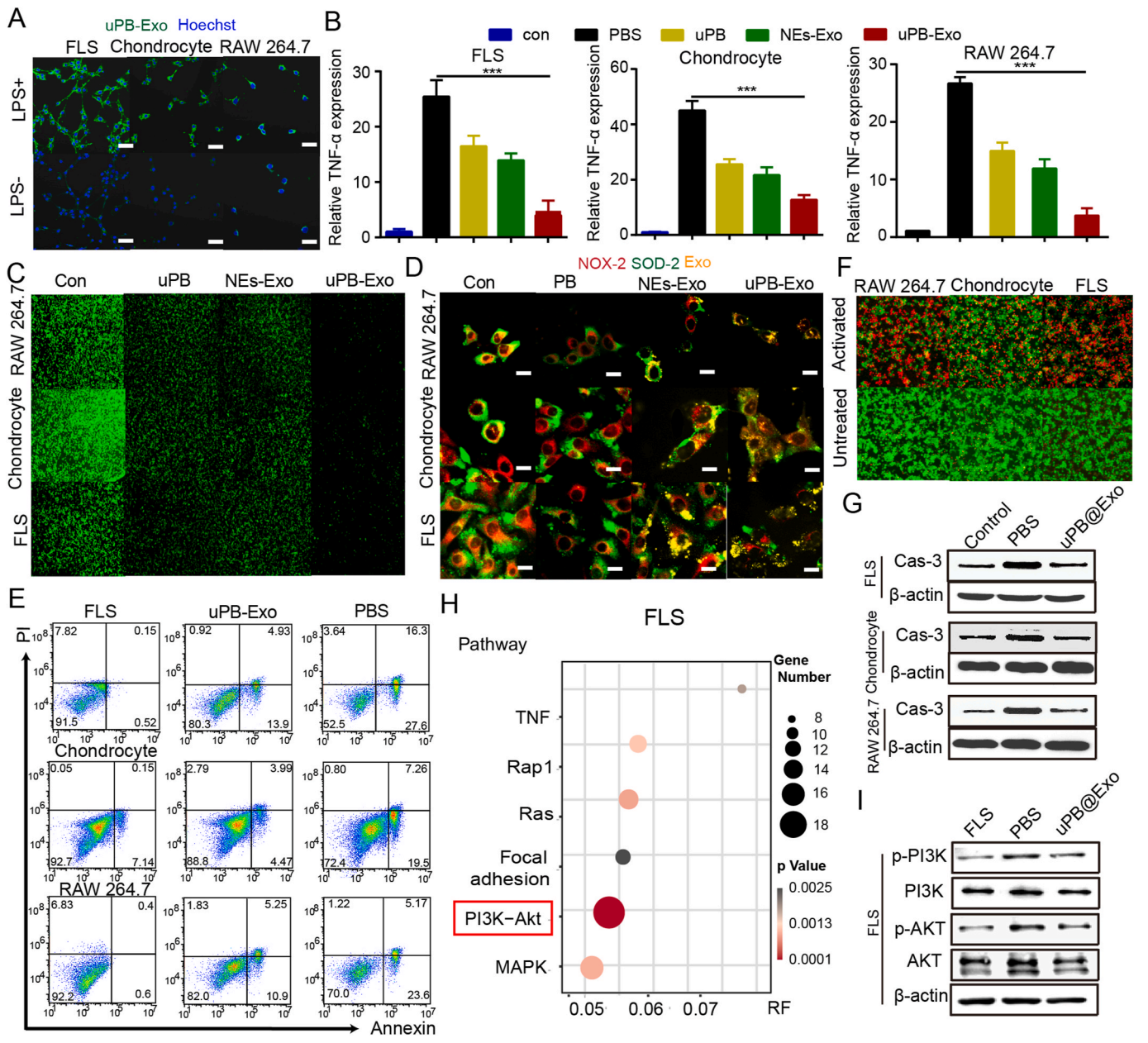

Fig. 4. Inflammatory environment regulation of uPB-Exo *in vitro*. (A) Confocal microscopic images of activated FLS, Chondrocyte, RAW264.7 cells incubated with DiO labeled uPB-Exo. The scale bars indicate 20 μm. Cells treated with PBS were used as control. (B) The relative expression of TNF-α in activated FLS, Chondrocyte, RAW264.7 cells incubated with activated uPB-Exo, NEs-Exo and uPB. Cells treated with PBS were used as control. (C) ROS scavenging capacity of different formulations in activated FLS, Chondrocyte, RAW264.7 cells. (D) Fig. S21. Immunofluorescence analyses of the expression of antioxidative factors of SOD-2 (green) and NOX-2 (red) in activated RAW264.7 cells, Chondrocyte, FLS pre-incubated with DiD labeled uPB-Exo (yellow), DiD labeled NEs-Exo (yellow) or uPB, respectively. FLS, Chondrocyte or RAW264.7 cells were pretreated with uPB-Exo, NEs-Exo, uPB or culture media for 4 h, then cells were treated with 2 μg/mL LPS for 12 h. LPS activated cells pretreated with culture media were used as control. (E) Flow cytometry analysis with Annexin V-PI staining was performed to evaluate the percentage of apoptotic cells in activated FLS, Chondrocyte, RAW264.7 cells incubated with uPB-Exo. (F) The live/dead stained of activated FLS, Chondrocyte, RAW264.7 cells incubated with uPB-Exo. (G) Protein expression levels of Cleaved Caspase-3 in activated FLS, Chondrocyte, RAW264.7 cells incubated with uPB-Exo detected by Western blot assay. (H) KEGG pathway analysis of activated FLS treated with uPB-Exo compared with PBS. Significance is indicated by color, and the number of DEGs is indicated by the size of a circle. (I) Protein expression levels of PI3K/AKT in activated FLS incubated with uPB-Exo detected by Western blot assay.

uPB-Exo and the intercellular activation molecule 1 (ICAM-1) overexpressed on activated FLS. The activated FLS in RA joints play important roles in synovial inflammation and joint destruction [39]. To investigate whether uPB-Exo could effectively decrease the inflammation in FLS, their expression profile of inflammation factors (TNF-α and IL-1β) was determined by Elisa kit. As shown in Figs. 4B and S18, both NEs-Exo and uPB demonstrated apparent anti-inflammation activities in activated FLS compared to control group. Particularly, uPB-Exo treatment exhibited the lowest expression of both TNF-α and IL-1β in activated FLS, compared to control groups. The anti-inflammatory ability of uPB-Exo were observed in activated Chondrocyte and RAW264.7 cells (Fig. 4B). These result indicating that uPB-Exo holds the great potential for ameliorating joint inflammation.

2.29. Anti-oxidative effects of uPB-Exo in vitro

ROS regulate the migration and invasion of FLS, and play a prominent role in the progression of RA. uPB own outstanding POD-like and

CAT-like activities, thereby endowing uPB-Exo with the great antioxidant activities for relieving oxidative stress [36]. We next examined the ROS level of activated cells pre-treated with uPB-Exo via flow cytometry assay (Fig. S19) and fluorescence microscopic imaging (Fig. 4C), staining with a ROS probe (DCFH-DA). Quantitative flow cytometry experiments showed that uPB-Exo demonstrated much better antioxidative effect than uPB under the same concentration (Fig. S19). In addition, the greatest decrease in green signals were observed in uPB-Exo treatments in activated FLS, Chondrocyte and RAW264.7 cells, indicating that uPB-Exo has good ROS elimination ability (Fig. 4C). Moreover, the expression of antioxidative factors expression level was also assessed by immunofluorescence staining. Superoxide dismutase 2 (SOD-2) and NADPH oxidase 2 (NOX-2) protein are well known biomarkers of oxidative stress [57,58]. SOD-2 is localized within mitochondria and efficiently eliminates the superoxide generated from molecular oxygen in the respiratory chain [59]. Many issues have reported that LPS caused a time- and dose-dependent manner in up-regulating SOD-2 protein expression, and the increased SOD-2 conferred oxidative stress tolerance on cells [60–62]. In addition, LPS treatment also could induce the production of ROS [63,64]. Considering the increased NOX-2 is an important indicator of ROS generation [58], these oxidative stress-related biomarkers (SOD-2 and NOX-2) were measured to further determine whether uPB-Exo could reduce oxidative stress in LPS-treated FLS. In previous studies, we found that LPS upregulates SOD-2 expression within 24 h in FLS, and the SOD-2 levels reached maximum values after 12 h-treatment (Fig. S20). These results indicated that elevated SOD-2 protein levels could protect FLS form subsequent challenges of oxidative stress induced by ROS. FLS were pretreated with uPB-Exo for 4 h, then cells were treated with 2 μg/mL LPS for 12 h to induce profound elevation of SOD-2 and NOX-2 expression. As shown in Fig. 4D, LPS treatment induced apparently SOD-2 expression in FLS after LPS treatment. However, pretreatment with uPB-Exo significantly reversed the improvement of SOD-2 by LPS treatment, which is 2.1-fold lower compared to NE-Exo groups (Figs. S21–S22). These results suggested that uPB-Exo can act as SOD-2 mimics with excellent protecting effects against oxidative stress. In addition, increasing expression of NOX-2 protein was also observed in FLS, Chondrocyte and RAW264.7 cells with only LPS treatment. After pretreated with uPB-Exo, the protein expression of the NOX-2 was notably decreased compared with uPB or NE-Exo groups, which are in good agreement with the ROS assay data. These results indicated that uPB-Exo can be used as an effective ROS scavenger to regulate oxidative microenvironment in inflamed joints.

2.30. *Protective effects of uPB-Exo against cytokine induced cell apoptosis in vitro*

It has been generally accepted that cytokine induced cell apoptosis displays a key role in pathogenesis of RA [48]. Pro-inflammatory cytokine TNF-α have been shown to induce the apoptosis of normal FLS cells *in vitro* and *in vivo* [65–68], resulted in cartilage matrix degradation and joint inflammation, thereby contributing to RA progression. Thus, our study used TNF-α to mimic an *in vitro* model of RA, and the cell apoptosis were measured via Annexin-V/PI flow cytometry. As shown in Figs. 4E and S23, after treated with uPB-Exo, the percentages of FLS cells in both early and late apoptosis states were significantly reduced compared to TNF-α stimulated groups. Since high level of proinflammatory cytokines activate apoptosis signaling and initiate cell death, we therefore evaluated the rescue of uPB-Exo for TNF-α-promoted cell death. uPB-Exo could significantly rescue the cell viability of FLS induced by TNF-α (Fig. S24). In addition, a live/dead kit assay was conducted to evaluate joint protection ability of uPB-Exo in activated FLS (Fig. 4F). Our study further confirmed pre-treatment with uPB-Exo could remarkably reduce the cell apoptosis in stimulated FLS induce by TNF-α. Importantly, to determine whether uPB-Exo can modulate the expression of apoptotic marker, we examined TNF-α-stimulated FLS with or without pre-treatment of uPB-Exo by Western blot (Fig. 4G). The expression of cleaved caspase-3 was increased in stimulated FLS compared to normal cells. However, uPB-Exo remarkably inhibited TNF-α-induced cleaved caspase-3 overexpression, indicating that uPB-Exo might have an anti-apoptotic effect on TNF-α-stimulated FLS via suppressing cleaved caspase-3 expression. Similar anti-apoptotic results were also observed in Chondrocyte and RAW264.7 cells (Fig. 4E–G). These results suggest that uPB-Exo has a joint protective effect on TNF-α-induced cell models via attenuating the oxidative stress in RA joints.

Since uPB-Exo has excellent protective effects against cytokine induced cell apoptosis, we therefore performed an RNA-Seq assay in combination with expression profiling using TNF-α stimulated FLS, Chondrocyte or RAW264.7 cells pretreated with or without uPB-Exo to unravel the underlying mechanisms for regulating the inflammatory microenvironment. Genome-wide analysis indicated that numerous modulatory genes were associated with FLS cellular fate after uPB-Exo treatment. We found that the inflammation related genes, including colony stimulating factor 3 [69,70], matrix metallopeptidase 9 [71], interleukin 1 alpha [72], interleukin 1 beta [72], interleukin 7 receptor [73] and Von Willebrand factor [74], were markedly downregulated in uPB-Exo groups (Fig. S25). Of note, their down-regulation indicated anti-inflammatory effects of uPB-Exo. Collected evidences have shown that the downregulated genes, including colony stimulating factor 3 [75], matrix metallopeptidase 9 [76], interleukin 1 alpha [77], interleukin 1 beta [78], interleukin 7 receptor [79] and Von Willebrand factor [80] could be regulated by PI3K/AKT pathway. Meanwhile, KEGG pathway enrichment analysis demonstrated that numerous down-regulated genes were significantly enriched PI3K-Akt pathway in FLS with uPB-Exo treatment (Fig. 4H). We therefore valuated the expression of PI3K/AKT and related proteins in FLS by Western blot analyses after RNA-Seq screening. As shown in Fig. 4I, TNF-α could induce the overexpression of *p*-AKT and AKT in FLS compared with control group. After treated with uPB-Exo, inhibited *p*-AKT and AKT expression were apparently observed. In consideration of the same result observed in apoptosis analysis (Fig. 4E), these results demonstrated that uPB-Exo may inhibit the apoptosis of FLS via regulating PI3K/AKT signaling pathway.

In addition, KEGG pathway analysis showed that NF-kB pathway participated in RAW264.7 cells after treated with uPB-Exo (Fig. S26A). As shown in Fig. S26B, the expression of p-P65 were activated after TNF-α treatment in RAW264.7 cells, implying the detrimental effect of NF-κB activation on RAW264.7 cells induced by TNF-α. However, the administration of uPB-Exo led to significant alleviation in terms of p-P65, indicating that the NF-κB pathway was inhibited by uPB-Exo to protect chondrocytes from TNF-α inflammation. Furthermore, mTOR pathway plays an important role in promoting the proliferation and survival of chondrocyte. To further clear the effect of uPB-Exo on the mTOR pathway in Chondrocyte, the phosphorylation level of mTOR were determined. Although the mTOR phosphorylated activation was not obviously increased after treated with TNF-α, uPB-Exo indeed decreased the phosphorylation of mTOR (Fig. S26C). Hence, uPB-Exo protected joint from damage in RA through the effective inhibition of cytokines-induced cell apoptosis, which making it a decisive option in the treatment against RA onset and development.

2.31. *Inflammation targeting ability of uPB-Exo*

Neutrophils-derived exosomes (NEs-Exo) are nano-sized (50–150 nm) mammalian extracellular particles with essential properties similar to neutrophils. Considering the inflammation targeting ability of NEs-Exo, the biodistribution of engineered exosomes in CIA mice model were further evaluated. In this work, CIA mice were i.v. injected with DiR@NEs-Exo, DiR@uPB-Exo or DiR dye, followed by imaging with IVIS Spectrum imaging system. Fig. 5A shows that both DiR@NEs-Exo and DiR@uPB-Exo exhibited the more accumulation into inflammation joints at every time point compared to DiR group (Fig. S27), and reaching the maximum fluorescence accumulation with 4 h post

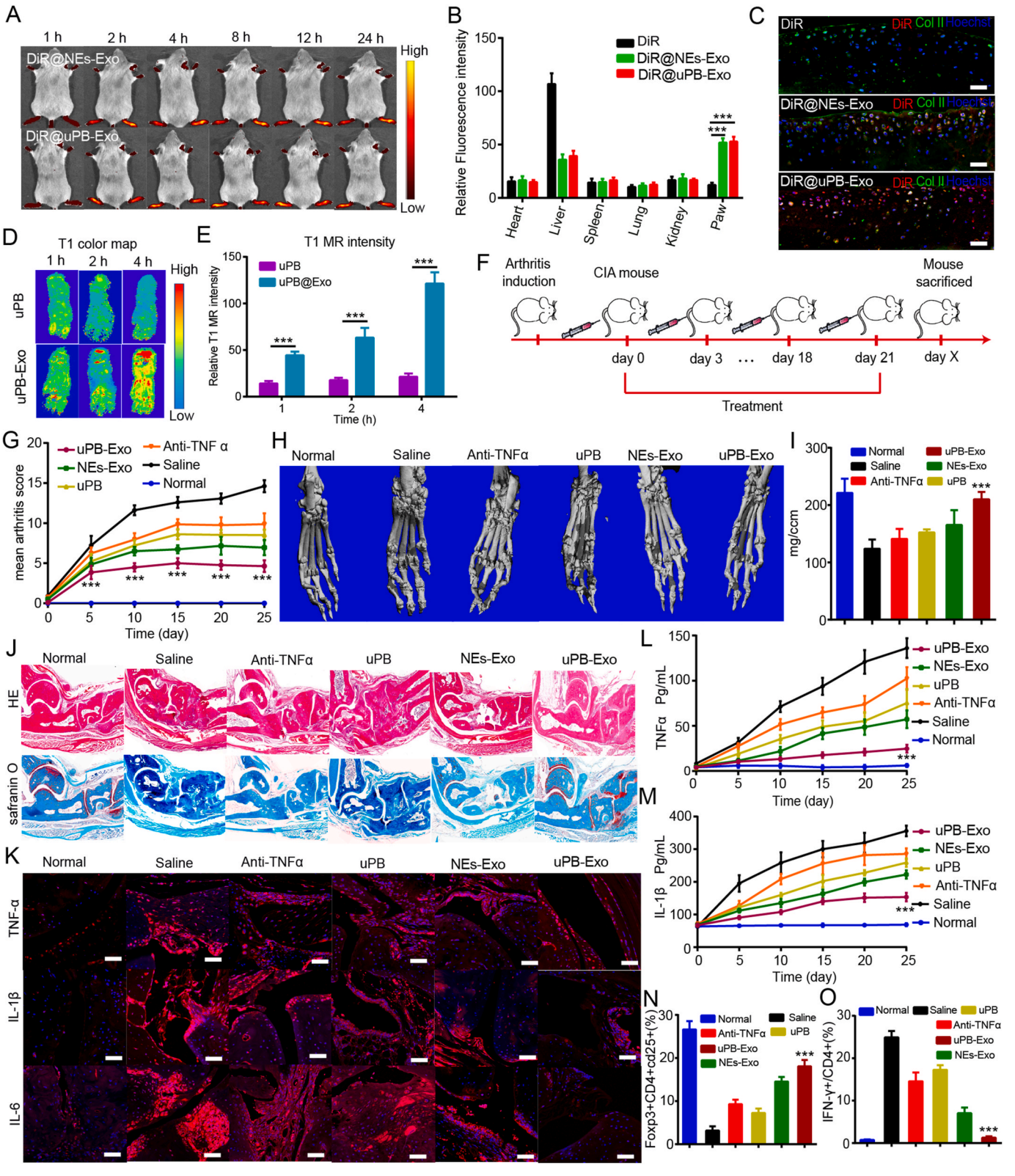

(caption on next page)

Fig. 5. The biodistribution and therapeutic treatment of uPB-Exo in advanced RA mouse model. (A) In vivo fluorescence imaging of CIA mice after intravenous injection of DiR@NEs-Exo or DiR@uPB-Exo. (B) The relative fluorescent signal ratios between RA inflammation ankle joint regions and normal tissues were measured at different time points after injected with DiR dye, DiR@NEs-Exo or DiR@uPB-Exo. Data expressed as mean ± SD, n = 3. ***P < 0.001, compared with controls (two-tailed Student's t-test). (C) Representative confocal images of the knee joints of mice after systemic administrated with DiR-labeled exosomes (Red signal) or DiR (Red signal) for 24 h. The cartilage region was stained with Collagen II antibody (Green signal), and Nuclei were stained with Hoechst (Blue signal). The Scale bars indicated 100 μm. (D). In vivo T1-weighted MR images of inflamed paws of CIA mice injected intravenously with uPB-Exo or uPB. (E) T2-weighted MR signal as a function of time for uPB-Exo or PB. Data expressed as mean ± SD, n = 3. ***P < 0.001, compared with controls (two-tailed Student's t-test). (F) The study protocol of a prophylactic regimen with a CIA mouse model. (G) Arthritis index in different groups over 25 days of treatment; n = 6, p-value, ***p < 0.001. (H) Representative micro-CT images of ankle joints from mice with different treatments. (I) Quantitative micro-CT analyses of bone mineral density (BMD). n = 6, p-value, ***p < 0.001. (J) Representative images of H&E staining and safranin-O staining on ankle joints from mice with different treatments. Images were acquired using a bright-light microscope (10 × magnification). (K) Immunofluorescence analyses of the TNF-α, IL-1β and IL-6 in the joint tissues from CIA mice treated with different groups. (L)(M) Concentration profiles of TNF-α (L) and IL-1β (M) in the serum of CIA mice treated with different groups. (N)(O) The expression of IFN-γ (N), and CD25+Foxp3+ (O) on $CD4^+$ T cells were measured in serum by flow cytometry. Data expressed as mean ± SD, n = 6. p-value, ***P < 0.001, compared with controls (two-tailed Student's t-test).

injection in the region of inflamed paws (Fig. S28), indicating that the engineered Exos have good RA targeting ability as well as NEs-Exo. In addition, DiR@uPB-Exo group displayed significantly fluorescence within 24 h post injection, and generating a 11.5-fold higher fluorescent signal compare to DiR group (Fig. S28), suggesting that uPB-Exo can improve inflammation joints accumulation with a long-period retention. Furthermore, *ex vivo* imaging shows that obvious fluorescence was detected in inflammation paws after treated with DiR@uPB-Exo, and lower distribution of DiR signal in liver were observed in DiR@uPB-Exo group compared to DiR group (Figs. 5B and S29), confirming that uPB-Exo has high selectivity toward inflammatory ankle joints.

Many studies have reported the good penetration ability of neutrophils in inflammation cartilage [33], we therefore investigated the distribution of uPB-Exo in cartilage penetration. Mouse femoral head explants were collected and cultured in medium containing IL-1β to mimic inflammatory arthritis. DiR labeled exosomes were administrated and cultured for 8 h of incubation. As shown in Fig. S30, notable accumulation of both DiR@uPB-Exo and DiR@NEs-Exo (red signal) were observed in Coll II labeled cartilage region (Green signal) compared to DiR group. Despite the surface of cartilage, DiR@uPB-Exo as well as DiR@NEs-Exo penetrated cartilage matrix deeply. The enhanced cartilage penetration of DiR@uPB-Exo is probably attributable to the adhesion interactions between NEs-Exo and chondrocytes. To further confirm whether DiR@uPB-Exo could accumulate in the cartilage region deeply, the fresh joints were collected after injected with DiR@uPB-Exo within 24 h. As shown in Fig. 5C, the confocal images showed that more DiR@uPB-Exo (red signal) was accumulated in the Coll II labeled cartilage region (green signal), exhibiting more yellow signal in RA cartilage region, as compared with DiR group, which suggested that DiR@uPB-Exo could penetrated cartilage matrix deeply *in vivo*. These results demonstrated the potential therapeutic effects of uPB-Exo for cartilage destruction.

Since uPB-Exo was a contrast agent for MRI, we also analyzed MR images of the CIA mice treated with uPB-Exo or uPB (Fig. 5D). In the control group, slight signals of uPBs were observed in the inflamed paws within 4 h after PBs injection. In contrast, the mice treated with uPB-Exo showed apparent amount of uPB accumulated in the inflamed paw, and generating 8.6-fold higher in T1 signals compared to uPB groups (Fig. 5E), which is consistent with the *in vivo* imaging experiments. These results confirmed that the modification of uPB on NEs-Exo can promote delivery of uPB to the inflamed paws and enhanced its retention, indicating that uPB-Exo has the great potential for effective treatment of RA.

2.32. Effective therapeutic effects of uPB-Exo in advanced RA

It has been reported that biodistribution determined the therapeutic efficacy of nanoscale therapeutics. Inspired by the excellent inflammation ankle targeting capability and good cartilage permeability, we therefore investigated the therapeutic efficacy of uPB-Exo in CIA mice model. Saline or various exosomes were intravenously injected into CIA mice (Fig. 5F). The CIA mice in advanced-stages developed severe swelling in the ankles and paws after 15 days of arthritis induction. The extent of paw swelling was used as a direct indicator for the treatment of RA. Thus, paw swelling was observed over time as an index of arthritis. As shown in Fig. 5G, free uPB and anti-TNF α group showed relatively low efficacy in decreasing the paw thickness and ankle diameters of CIA mice with advanced arthritis. In addition, increased swelling was observed in free uPB and anti-TNF-α group, compared to normal mice. In contrast, uPB-Exo and NEs-Exo showed higher efficacy in reducing swelling in ankle joints and paws (Fig. 5H and I). Significantly, uPB-Exo group showed an ankle diameter and paw thickness closer to that of the normal group at the study endpoint (Figs. S31 and S32). These results indicated that uPB-Exo has excellent therapeutic effects for RA, holding great potential for the treatment of RA in clinic.

To further confirm that uPB-Exo could relief joint inflammation and reduce cartilage destructions, the ankle joints of mice were sectioned for histological analysis at the study endpoint. As show in Fig. 5J, HE stained sections from the saline group displayed severe synovial hyperplasia, along with bone and cartilage destruction. The free uPB and anti-TNF-α group exhibited a limited effect in reducing these symptoms, while uPB-Exo can not only reduce synovial inflammation but also decrease the loss of cartilage to some extent compared with the saline group (Fig. 5J). In addition, safranin-O staining indicated that the GAG levels in uPB-Exo were higher than those control group, suggesting that the cartilage damage was efficiently reversed and prevented progressive. Importantly, the uPB-Exo group had larger positive areas for safranin-O staining, which were closer to those of the normal group, suggesting effective therapeutic effects for RA. These results demonstrated that uPB-Exo can alleviate synovial inflammation and reduce cartilage destructions in CIA mice with advanced arthritis, holding the great potential in the treatment of RA in clinic.

Collected evidence have shown that the therapeutic effects on rheumatoid arthritis have been positively associated with a decrease expression of proinflammatory cytokines. Therefore, the changes of proinflammatory cytokine expression were evaluated after the treatments of uPB-Exo. As shown in Fig. 5K, the expression of proinflammatory cytokines, including TNF-α, IL-1β and IL-6, were significantly elevated in the saline group compared with normal mice group, indicating the important involvement of these cytokines in the pathogenesis of RA. In addition, no significant differences in the expression of these cytokines were observed in both anti-TNF-α group and uPB group compared with saline group. Whereas, the expression levels of the proinflammatory cytokines, including TNF-α, IL-1β and IL-6, were decreased in the uPB-Exo group. In addition, the levels of proinflammatory cytokines in serum, including TNF-α and IL-1β, were also monitored during the treatments of uPB-Exo. As shown in Fig. 5L and M, uPB-Exo exhibited obviously anti-inflammatory ability compared to other treatments. These results demonstrated that the administration of uPB-Exo to CIA mice with advanced RA could remarkably reduce the production of proinflammatory cytokines, presumably contributing to the therapeutic effect against RA.

2.33. Immune-regulation of uPB-Exo in CIA mice with advanced stage

Considering that Th17/Treg balances play a pivotal role in RA pathology [81,82], we next investigated the impact of uPB-Exo on these effector cells. To determine whether the Th17 and Treg cell populations were altered in uPB-Exo-treated CIA mice, the ratios of $CD4^+$ IL-17^+ cells (Th17 cells) and $CD4^+$ Foxp3 $^+$ cells (Tregs) in the $CD4^+$ T cells were assessed by flow cytometry (Figs. S33 and S34). Compared to health mice, uPB-Exo-treated CIA mice exhibited up-regulated $CD4^+$ IL-17+ cells and down-regulated $CD4^+$ Foxp3+ cells, suggesting the increased of Th17 cell population and decreased Treg cell population (Fig. 5N and O), indicating that Th17 cell/Treg imbalances associated with arthritis were rescued by uPB-Exo treatment. Importantly, uPB-Exo showed good biocompatibility, and no noticeable changes in the body weight and systemic toxicity were observed (Figs. S35 and S36). These results indicated that uPB-Exo induced a cascade of anti-inflammatory events via Th17/Treg cell balance regulation, thereby providing a promising strategy for RA in clinic.

3. Conclusions

In summary, we have developed a neutrophil-derived exosomes engineered with sub-5 nm ultrasmall PBNPs (uPB) via click chemistry, termed as uPB-Exo, which could selectively neutralize pro-inflammatory factors and alleviate oxidative stress in activated fibroblast-like synoviocytes (FLS), macrophages and chondrocytes. uPB-Exo effectively targeted to inflammation synovitis, and penetrated into cartilage deeply. In addition, uPB-Exo could significantly ameliorate joint damage and suppress overall arthritis severity in CIA mice via Th17/Treg cell balance regulation in advanced RA mouse model. Therefore, the engineered exosomes displayed considerable potential for the clinical diagnosis and treatment of RA.

CRediT authorship contribution statement

Lei Zhang: Investigation, Data curation, Writing – original draft. **Zhiguo Qin:** Data curation, Formal analysis. **Han Sun:** Data curation, Formal analysis. **Xiang Chen:** Data curation, Formal analysis. **Jian Dong:** Data curation, Formal analysis, Data curation, Formal analysis. **Siyu Shen:** Data curation, Formal analysis. **Liming Zheng:** Data curation, Formal analysis. **Ning Gu:** Investigation, Data curation, Formal analysis, Conceptualization, Supervision. **Qing Jiang:** Investigation, Data curation, Formal analysis, Conceptualization, Supervision.

Conflict of interest

The authors declared that they have no conflicts of interest to this work.

Acknowledgments

Key Program of NSFC (81730067), Major Project of NSFC (81991514), Fundamental Research Funds for the Central Universities (14380493, 14380494), National Science Foundation of China (Grant No 82002370, 31800806, 82000069),China Postdoctoral Science Foundation (Grant No 2019M661806), Natural science foundation of Jiangsu province (Grant No BK20200117, BK20200314), Jiangsu postdoctoral research support project (Grant No 2021K059A), Nanjing University Innovation Program for PhD candidates (CXYJ21-62), Jiangsu Provincial Key Medical Center Foundation, Jiangsu Provincial Medical Outstanding Talent Foundation, Jiangsu Provincial Medical Youth Talent Foundation, Jiangsu Provincial Key Medical Talent Foundation, Program of Innovation and Entrepreneurship of Jiangsu Province.

Appendix A. Supplementary data

Supplementary data to this article can be found online at https://doi.org/10.1016/j.bioactmat.2022.02.017.

References

[1] D. Aletaha, J.S. Smolen, Diagnosis and management of rheumatoid arthritis: a review, JAMA 320 (2018) 1360–1372.
[2] G.S. Firestein, Evolving concepts of rheumatoid arthritis, Nature 423 (2003) 356–361.
[3] I.B. McInnes, G. Schett, The pathogenesis of rheumatoid arthritis, N. Engl. J. Med. 365 (2011) 2205–2219.
[4] L. Nerurkar, S. Siebert, I.B. McInnes, J. Cavanagh, Rheumatoid arthritis and depression: an inflammatory perspective, Lancet Psychiatr. 6 (2019) 164–173.
[5] Z. Chen, A. Bozec, A. Ramming, G. Schett, Anti-inflammatory and immune-regulatory cytokines in rheumatoid arthritis, Nat. Rev. Rheumatol. 15 (2019) 9–17.
[6] D.R. Lu, A.N. McDavid, S. Kongpachith, N. Lingampalli, J. Glanville, C.H. Ju, R. Gottardo, W.H. Robinson, T cell–dependent affinity maturation and innate immune pathways differentially drive autoreactive B cell responses in rheumatoid arthritis, Arthritis Rheumatol. 70 (2018) 1732–1744.
[7] S. Singh, T.G. Singh, K. Mahajan, S. Dhiman, Pharmacology, Medicinal plants used against various inflammatory biomarkers for the management of rheumatoid arthritis, J. Pharm. Pharmacol. 72 (2020) 1306–1327.
[8] E. Morand, M. Leech, J. Bernhagen, MIF: a new cytokine link between rheumatoid arthritis and atherosclerosis, Nat. Rev. Drug Discov. 5 (2006) 399–411.
[9] B. Friedman, B. Cronstein, Methotrexate mechanism in treatment of rheumatoid arthritis, Joint Bone Spine 86 (2019) 301–307.
[10] C.J. Lucas, S.B. Dimmitt, J.H. Martin, Optimising low-dose methotrexate for rheumatoid arthritis-A review, Br. J. Clin. Pharmacol. 85 (2019) 2228–2234.
[11] E.G. Favalli, M.G. Raimondo, A. Becciolini, C. Crotti, M. Biggioggero, R.J. Caporali, The management of first-line biologic therapy failures in rheumatoid arthritis: current practice and future perspectives, Autoimmun. Rev. 16 (2017) 1185–1195.
[12] C.J. Wruck, A. Fragoulis, A. Gurzynski, L. Brandenburg, Y.W. Kan, K. Chan, J. Hassenpflug, S. Freitag-Wolf, D. Varoga, S. Lippross, T. Pufe, Role of oxidative stress in rheumatoid arthritis: insights from the Nrf2-knockout mice, ARD (Ann. Rheum. Dis.) 70 (2011) 844–850.
[13] P. Vasanthi, G. Nalini, G. Rajasekhar, Status of oxidative stress in rheumatoid arthritis, Int. J. Rheum. Dis. 12 (2009) 29–33.
[14] L.K. Stamp, I. Khalilova, J.M. Tarr, R. Senthilmohan, R. Turner, R.C. Haigh, P. G. Winyard, A.J. Kettle, Myeloperoxidase and oxidative stress in rheumatoid arthritis, Rheumatology 51 (2012) 1796–1803.
[15] P.P. Tak, N.J. Zvaifler, D.R. Green, G. Firestein, Rheumatoid arthritis and p53: how oxidative stress might alter the course of inflammatory diseases, Immunol. Today 21 (2000) 78–82.
[16] J. Kim, H.Y. Kim, S.Y. Song, S. Go, H.S. Sohn, S. Baik, M. Soh, K. Kim, D. Kim, H. C. Kim, N. Lee, B. Kim, T. Hyeon, Synergistic oxygen generation and reactive oxygen species scavenging by manganese ferrite/ceria co-decorated nanoparticles for rheumatoid arthritis treatment, ACS Nano 13 (2019) 3206–3217.
[17] Y. He, Y. Yue, X. Zheng, K. Zhang, S. Chen, Z. Du, Curcumin, inflammation, and chronic diseases: how are they linked? Molecules 20 (2015) 9183–9213.
[18] T.H. Chou, D.S. Nugroho, J.Y. Chang, Y.S. Cheng, C.H. Liang, M.J. Deng, Encapsulation and characterization of nanoemulsions based on an anti-oxidative polymeric amphiphile for topical apigenin delivery, Polymers 13 (2021) 1016.
[19] M.T. Nurmohamed, B. Dijkmans, Efficacy, tolerability and cost effectiveness of disease-modifying antirheumatic drugs and biologic agents in rheumatoid arthritis, Drugs 65 (2005) 661–694.
[20] B.B. Aggarwal, G. Sethi, V. Baladandayuthapani, S. Krishnan, S. Shishodia, Targeting cell signaling pathways for drug discovery: an old lock needs a new key, J. Cell. Biochem. 102 (2007) 580–592.
[21] M. Vázquez-González, R.M. Torrente-Rodríguez, A. Kozell, W.C. Liao, A. Cecconello, S. Campuzano, J.M. Pingarrón, I. Willner, Mimicking peroxidase activities with prussian blue nanoparticles and their cyanometalate structural analogues, Nano Lett. 17 (2017) 4958–4963.
[22] W. Zhang, S. Hu, J.J. Yin, W.W. He, W. Lu, M. Ma, N. Gu, Y. Zhang, Prussian blue nanoparticles as multienzyme mimetics and reactive oxygen species scavengers, JACS 138 (2016) 5860–5865.
[23] X. Xie, J. Zhao, W. Gao, J. Chen, B. Hu, X. Cai, Y. Zheng, Prussian blue nanozyme-mediated nanoscavenger ameliorates acute pancreatitis via inhibiting TLRs/NF-κB signaling pathway, Theranostics 11 (2021) 3213–3228.
[25] M.A. Komkova, E.E. Karyakina, A.A. Karyakin, Catalytically synthesized prussian blue nanoparticles defeating natural enzyme peroxidase, JACS 140 (2018) 11302–11307.
[26] H.Y. Bai, T. Wang, F. Kong, M.C. Zhang, Z.X. Li, L.L. Zhuang, M. Ma, F.Z. Liu, C. Wang, H.Y. Xu, N. Gu, Y. Zhang, CXCR4 and CD44 dual-targeted Prussian blue nanosystem with daunorubicin loaded for acute myeloid leukemia therapy, Chem. Eng. J. 405 (2021), 126891.
[27] D.G. You, G.T. Lim, S. Kwon, W. Um, B.H. Oh, S.H. Song, J. Lee, D.G. Jo, Y.W. Cho, J.H. Park, Metabolically engineered stem cell-derived exosomes to regulate macrophage heterogeneity in rheumatoid arthritis, Sci. Adv. 7 (2021), eabe0083.
[28] H.L. Wright, R.J. Moots, S.W. Edwards, The multifactorial role of neutrophils in rheumatoid arthritis, Nat. Rev. Rheumatol. 10 (2014) 593–601.
[29] Q.Z. Zhang, D. Dehaini, Y. Zhang, J. Zhou, X.Y. Chen, L.F. Zhang, R.H. Fang, W. W. Gao, L.F. Zhang, Neutrophil membrane-coated nanoparticles inhibit synovial

inflammation and alleviate joint damage in inflammatory arthritis, Nat. Nanotechnol. 13 (2018) 1182–1190.
[30] S.E. Headland, H.R. Jones, L.V. Norling, A. Kim, P.R. Souza, E. Corsiero, C.D. Gil, A. Nerviani, F.D. Accio, C. Pitzalis, S.M. Oliani, L.Y. Jan, M. Perretti, Neutrophil-derived microvesicles enter cartilage and protect the joint in inflammatory arthritis, Sci. Transl. Med. 7 (2015), 315ra190-315ra190.
[31] C. Théry, L. Zitvogel, S. Amigorena, Exosomes: composition, biogenesis and function, Nat. Rev. Immunol. 2 (2002) 569–579.
[32] R. Kalluri, V.S. LeBleu, The biology, function, and biomedical applications of exosomes, Science 367 (2020) 1–15.
[33] D. Sun, X. Zhuang, X. Xiang, Y. Liu, S. Zhang, C. Liu, S. Barnes, W. Grizzle, D. Miller, H.G. Zhang, A novel nanoparticle drug delivery system: the anti-inflammatory activity of curcumin is enhanced when encapsulated in exosomes, Mol. Ther. 18 (2010) 1606–1614.
[34] J. Xue, Z. Zhao, L. Zhang, L. Xue, S. Shen, Y. Wen, Z. Wei, L. Wang, L. Kong, H. Sun, C. Zhang, Neutrophil-mediated anticancer drug delivery for suppression of postoperative malignant glioma recurrence, Nat. Nanotechnol. 12 (2017) 692–700.
[35] L. Zhang, Y. Zhang, Y. Xue, Y. Wu, Q. Wang, L. Xue, C. Zhang, Transforming weakness into strength: photothermal-therapy-induced inflammation enhanced cytopharmaceutical chemotherapy as a combination anticancer treatment, Adv. Mater. 31 (2019), 1805936.
[36] M. Abbasi, M.J. Mousavi, S. Jamalzehi, R. Alimohammadi, M.H. Bezvan, H. Mohammadi, S. Aslani, Strategies toward rheumatoid arthritis therapy; the old and the new, J. Cell. Physiol. 234 (2019) 10018–10031.
[37] M. Feldmann, Development of anti-TNF therapy for rheumatoid arthritis, Nat. Rev. Immunol. 2 (2002) 364–371.
[38] C. Roubille1, V. Richer, T. Starnino, C. McCourt, A. McFarlane, P. Fleming, S. Siu, J. Kraft, C. Lynde, J. Pope, W. Gulliver, S. Keeling, J. Dutz, L. Bessette, R. Bissonnette, B. Haraoui, The effects of tumour necrosis factor inhibitors, methotrexate, non-steroidal anti-inflammatory drugs and corticosteroids on cardiovascular events in rheumatoid arthritis, psoriasis and psoriatic arthritis: a systematic review and meta-analysis, ARD (Ann. Rheum. Dis.) 74 (2015) 480–489.
[39] J. Li, L. Chen, X. Xu, Y. Fan, X. Xue, M. Shen, X. Shi, Targeted combination of antioxidative and anti-inflammatory therapy of rheumatoid arthritis using multifunctional Dendrimer-Entrapped gold nanoparticles as a platform, Small 16 (2020), 2005661.
[40] Y. Yang, L. Guo, Z. Wang, P. Liu, X. Liu, J. Ding, W. Zhou, Targeted silver nanoparticles for rheumatoid arthritis therapy via macrophage apoptosis and Re-polarization, Biomaterials 264 (2021), 120390.
[41] R. Ni, G. Song, X. Fu, R. Song, L. Li, W. Pu, J. Gao, J. Hu, Q. Liu, F. He, D. Zhang, G. Huang, Reactive oxygen species-responsive dexamethasone-loaded nanoparticles for targeted treatment of rheumatoid arthritis via suppressing the iRhom2/TNF-α/BAFF signaling pathway, Biomaterials 232 (2020), 119730.
[42] M. Lu, Y. Huang, Bioinspired exosome-like therapeutics and delivery nanoplatforms, Biomaterials 242 (2020), 119925.
[43] J.S. Smolen, D. Aletaha, Rheumatoid arthritis therapy reappraisal: strategies, opportunities and challenges, Nat. Rev. Rheumatol. 11 (2015) 276–289.
[44] C. Weyand, J. Goronzy, Immunometabolism in early and late stages of rheumatoid arthritis, Nat. Rev. Rheumatol. 13 (2017) 291–301.
[45] Z. Qin, B. Chen, Y. Mao, C. Shi, Y. Li, X. Huang, F. Yang, N. Gu, Achieving ultrasmall prussian blue nanoparticles as high-performance biomedical agents with multifunctions, ACS Appl. Mater. Interfaces 12 (2020) 57382–57390.
[46] T. Tian, H.X. Zhang, C.P. He, S. Fan, Y.L. Zhu, C. Qi, N.P. Huang, Z.D. Xiao, Z.H. Lu, B.A. Tannous, J. Gao, Surface functionalized exosomes as targeted drug delivery vehicles for cerebral ischemia therapy, Biomaterials 150 (2018) 137–149.
[47] D. Brand, K. Latham, E. Rosloniec, Collagen-induced arthritis, Nat. Protoc. 2 (2007) 1269–1275.
[48] C.D. Buckley, C. Ospelt, S. Gay, K.S. Midwood, Location, location, location: how the tissue microenvironment affects inflammation in RA, Nat. Rev. Rheumatol. 17 (2021) 1–18.
[49] K.D. Metzler, T.A. Fuchs, W.M. Nauseef, D. Reumaux, J. Roesler, I. Schulze, V. Wahn, V. Papayannopoulos, A. Zychlinsky, Myeloperoxidase is required for neutrophil extracellular trap formation: implications for innate immunity, Blood 117 (2011) 953–959.
[50] A. Familtseva, N. Jeremic, S.C. Tyagi, Exosomes: cell-created drug delivery systems, Mol. Cell. Biochem. 459 (2019) 1–6.
[51] W. Huang, L. Zhang, C. Cheng, W. Shan, R. Ma, Z. Yin, C. Zhu, Parallel comparison of fibroblast-like synoviocytes from the surgically removed hyperplastic synovial tissues of rheumatoid arthritis and osteoarthritis patients, Bmc. Musculoskel. Discord. 20 (2019) 1–9.
[52] C. Pirozzi, V. Francisco, F. Di Guida, R. Gómez, F. Lago, J. Pino, R. Meli, O. Gualillo, Butyrate modulates inflammation in chondrocytes via GPR43 receptor, Cell. Physiol. Biochem. 51 (2018) 228–243.
[53] P.J. Dalal, R. Sumagin, Emerging functions of ICAM-1 in macrophage efferocytosis and wound healing, J. Cell. Immunol. 2 (2020) 250–253.
[54] H.L. Wright, R.J. Moots, S.W. Edwards, The multifactorial role of neutrophils in rheumatoid arthritis, Nat. Rev. Rheumatol. 10 (2014) 593–601.
[55] B.T. Wipke, P.M. Allen, Essential role of neutrophils in the initiation and progression of a murine model of rheumatoid arthritis, J. Immunol. 167 (2001) 1601–1608.
[56] Z.G. Qin, Y. Li, N. Gu, Progress in applications of Prussian blue nanoparticles in biomedicine, Adv. Healthc. Mater. 7 (2018), 1800347.
[57] T. Fukai, M. Ushio-Fukai, Superoxide dismutases: role in redox signaling, vascular function, and diseases, Antioxidants Redox Signal. 15 (2011) 1583–1606.
[58] A. Tarafdar, G. Pula, The role of NADPH oxidases and oxidative stress in neurodegenerative disorders, Int. J. Mol. Sci. 19 (2018) 3824.
[59] Y. Ishihara, T. Takemoto, K. Itoh, A. Ishida, T. Yamazaki, Dual role of superoxide dismutase 2 induced in activated microglia: oxidative stress tolerance and convergence of inflammatory responses, J. Biol. Chem. 290 (2015) 22805–22817.
[60] C. Li, D. Ma, M. Chen, L. Zhang, L. Zhang, J. Zhang, J. Zhang, X. Qu, C. Wang, Ulinastatin attenuates LPS-induced human endothelial cells oxidative damage through suppressing JNK/c-Jun signaling pathway, Biochem. Biophys. Res. Commun. 474 (2016) 572–578.
[61] D.H. Yu, J.K. Yi, H.S. Yuh, H.J. Kim, K.B. Bae, Y.R. Ji, N.R. Kim, S.J. Park, D. H. Kim, S.H. Kim, M.O. Kim, J.W. Lee, Z.Y. Ryoo1, Over-expression of extracellular superoxide dismutase in mouse synovial tissue attenuates the inflammatory arthritis, Exp. Mol. Med. 44 (2012) 529–535.
[62] Z. Qu, F. Meng, H. Zhou, J. Li, Q. Wang, F. Wei, J. Cheng, C.M. Greenlief, D. B. Lubahn, G.Y. Sun, S. Liu, Z. Gu, NitroDIGE analysis reveals inhibition of protein S-nitrosylation by epigallocatechin gallates in lipopolysaccharide-stimulated microglial cells, J. Neuroinflammation 11 (2014) 1–13.
[63] T. Wang, L. Qin, B. Liu, Y. Liu, B. Wilson, T.E. Eling, R. Langenbach, S. Taniura, J. S. Hong, Role of reactive oxygen species in LPS-induced production of prostaglandin E2 in microglia, J. Neurochem. 88 (2004) 939–947.
[64] J. Park, J.S. Min, B. Kim, U.B. Chae, J.W. Yun, M.S. Choi, I.K. Kong, K.T. Chang, D. S. Lee, Mitochondrial ROS govern the LPS-induced pro-inflammatory response in microglia cells by regulating MAPK and NF-κB pathways, Neurosci. Lett. 584 (2015) 191–196.
[65] S. Li, J.W. Chen, X. Xie, J. Tian, C. Deng, J. Wang, H.N. Gan, F. Li, Autophagy inhibitor regulates apoptosis and proliferation of synovial fibroblasts through the inhibition of PI3K/AKT pathway in collagen-induced arthritis rat model, Am. J. Transl. Res. 9 (2017) 2065.
[66] C.K. Wong, D.P. Chen, L.S. Tam, K.L. Edmund, Y.B. Yi, W.L. Christopher, Effects of inflammatory cytokine IL-27 on the activation of fibroblast-like synoviocytes in rheumatoid arthritis, Arthritis Res. Ther. 12 (2010) 1–15.
[67] W. Jing, W. Sun, N. Zhang, C. Zhao, X. Yan, The protective effects of the GPR39 agonist TC-G 1008 against TNF-α-induced inflammation in human fibroblast-like synoviocytes (FLSs), Eur. J. Pharmacol. 865 (2019), 172663.
[68] M. Peng, L. Qiang, Y. Xu, C. Li, T. Li, J. Wang, IL-35 ameliorates collagen-induced arthritis by promoting TNF-α-induced apoptosis of synovial fibroblasts and stimulating M2 macrophages polarization, FEBS J. 286 (2019) 1972–1985, 2019.
[69] P. Mehta, J.C. Porter, J.J. Manson, J.D. Isaacs, P.J.M. Openshaw, I.B. McInnes, C. Summers, R.C. Chambers, Therapeutic blockade of granulocyte macrophage colony-stimulating factor in COVID-19-associated hyperinflammation: challenges and opportunities, Lancet Respir. Med. 8 (2020) 822–830.
[70] J.A. Hamilton, GM-CSF-dependent inflammatory pathways, Front. Immunol. 10 (2019) 2055.
[71] J. Park, S.H. Ha, F. Abekura, H. Lim, J. Magae, K.T. Ha, T.W. Chung, Y.C. Chang, Y. C. Lee, E. Chung, J. Ku, C.H. Kim, 4-O-Carboxymethylascochlorin inhibits expression levels of on inflammation-related cytokines and matrix metalloproteinase-9 through NF–κB/MAPK/TLR4 signaling pathway in LPS-activated RAW264. 7 cells, Front. Pharmacol. 10 (2019) 30.
[72] A. Mantovani, C.A. Dinarello, M. Molgora, C. Garlanda, Interleukin-1 and related cytokines in the regulation of inflammation and immunity, Immunity 50 (2019) 778–795.
[73] A. Shimba, G. Cui, S. Tani-Ichi, M. Ogawa, S. Abe, F. Okazaki, S. Kitano, H. Miyachi, H. Yamada, T. Hara, Y. Yoshikai, T. Nagasawa, G. Schütz, K. Ikuta, Glucocorticoids drive diurnal oscillations in T cell distribution and responses by inducing interleukin-7 receptor and CXCR4, Immunity 48 (2018) 286–298.
[74] J. Chen, D.W. Chung, Inflammation, von Willebrand factor, and ADAMTS13, Blood 132 (2018) 141–147.
[75] C.C. Mandal, G.G. Choudhury, N. Ghosh-Choudhury, Phosphatidylinositol 3 kinase/Akt signal relay cooperates with smad in bone morphogenetic protein-2-induced colony stimulating factor-1 (CSF-1) expression and osteoclast differentiation, Endocrinology 150 (2009) 4989–4998.
[76] P. Teng, Y. Liu, Y. Dai, H. Zhang, W.T. Liu, J. Hu, Nicotine attenuates osteoarthritis pain and matrix metalloproteinase-9 expression via the α7 nicotinic acetylcholine receptor, J. Immunol. 203 (2019) 485–492.
[77] J. Ma, X. Sun, T. Guo, H. Su, Q. Chen, Z. Gong, J. Qi, X. Zhao, Interleukin-1 receptor antagonist inhibits angiogenesis via blockage IL-1α/PI3K/NF-κβ pathway in human colon cancer cell, Cancer Manag. Res. 9 (2017) 481–493.
[78] L. Yang, X.G. Guo, C.Q. Du, J.X. Yang, D.M. Jiang, B. Li, W.J. Zhou, F.R. Zhang, Interleukin-1 beta increases activity of human endothelial progenitor cells: involvement of PI3K-Akt signaling pathway, Inflammation 35 (2012) 1242–1250.
[79] M. Jian, Z. Yunjia, D. Zhiying, J. Yanduo, J. Guocheng, Interleukin 7 receptor activates PI3K/Akt/mTOR signaling pathway via downregulation of Beclin-1 in lung cancer, Mol. Carcinog. 58 (2019) 358–365.
[80] J. Fang, X. Sun, S. Liu, P. Yang, J. Lin, J. Feng, M.A. Cruz, J. Dong, Y. Fang, J. Wu, Shear Stress Accumulation enhances von Willebrand factor-induced platelet P-selectin translocation in a PI3K/Akt pathway-dependent manner, Front. Cell Dev. Biol. 9 (2021) 64218.
[81] S. Jin, H. Chen, Y. Li, H. Zhong, W. Sun, J. Wang, T. Zhang, J. Ma, S. Yan, J. J. Zhang, Maresin 1 improves the Treg/Th17 imbalance in rheumatoid arthritis through miR-21, ARD (Ann. Rheum. Dis.) 77 (2018) 1644–1652.
[82] C.H. Evans, V.B. Kraus, L.A. Setton, Progress in intra-articular therapy, Nat. Rev. Rheumatol. 10 (2014) 11–22.